

Electronic Supplementary Information

Experimental section

Materials: Cobaltous(II) nitrate hexahydrate ($\text{Co}(\text{NO}_3)_2 \cdot 6\text{H}_2\text{O}$), p-phthalic acid ($\text{C}_8\text{H}_6\text{O}_4$), urea ($\text{CH}_4\text{N}_2\text{O}$), ammonium fluoride (NH_4F), hydrochloric acid (HCl), potassium hydroxide (KOH) and sodium hypophosphite ($\text{NaH}_2\text{PO}_2 \cdot \text{H}_2\text{O}$) were purchased from Jinan Camolai Trading Company. Nickel foam (NF) was provided by Hongshan District, Wuhan Instrument Surgical Instruments business. Pt/C (20 wt% Pt on Vulcan XC-72R) and RuO_2 were purchased from Jinan Jiadong Chemical Co., Ltd.. The ultrapure water (UP H_2O) was obtained by AD3L-05-030OR UP H_2O instrument. All chemicals are analytically pure without further purification.

Preparation of Co(OH)F/NF: First, 40 ml of ultrapure water, 2 mmol of cobaltous(II) nitrate hexahydrate ($\text{Co}(\text{NO}_3)_2 \cdot 6\text{H}_2\text{O}$), 5 mmol of ammonium fluoride (NH_4F) and 10 mmol of urea ($\text{CH}_4\text{N}_2\text{O}$) were placed in a beaker and stirred for 30 minutes to form a homogeneous solution. Then, this pink solution and a piece of pre-treated NF with a metallic luster were poured into a Teflon-lined autoclave and heated to 120 °C for 6 h. Finally, the product was cooled to room 25 °C, washed with ultrapure water and dried in a vacuum oven at 50 °C.

Synthesis of Co-MOF/NF: A piece of Co(OH)F/NF and p-phthalic acid ($\text{C}_8\text{H}_6\text{O}_4$, 100 mg) were placed at the center and upstream sides of the tube furnace, respectively. Then, the temperature was raised to 350 °C at a rate of 5 °C min^{-1} and held for 2 h in an atmosphere of Ar, yielding Co-MOF/NF catalyst after natural cooling.

Synthesis of p-CoP/NF: A piece of Co-MOF/NF and 500 mg NaH_2PO_2 (at the upstream side of the furnace) were placed in two separate quartz boats, heated to 280 °C at a rate of 2 °C min^{-1} and maintained for 2 h under a flowing Ar atmosphere. After cooling to room temperature, p-CoP/NF catalyst was obtained. By comparing the mass of bare NF and p-CoP/NF, the loading of p-CoP/NF is about 1.25 mg cm^{-2} .

Synthesis of CoP/NF: The as-obtained Co(OH)F/NF sample and 500 mg NaH_2PO_2 powder were placed in the central and upstream positions of a tube furnace, respectively. The temperature was increased to 280 °C within 2 h and hold for 2 h under

Ar gas. After the furnace was naturally cooled down to room temperature, Co(OH)F was converted to CoP, yielding a CoP/NF sample. According to the same calculation, the loading of CoP/NF is about 1.1 mg cm⁻².

Characterizations: Scanning electron microscopy (SEM) images and energy dispersive spectroscopy (EDS) was obtained from a field emission SEM (ZEISS, Germany) with an accelerating voltage of 20 kV. Transmission electron microscopy (TEM), high-resolution TEM (HRTEM) data and selected area electron diffraction (SAED) pattern were performed on JEOL JEM-2100 electron microscopy (Tokyo, Japan). X-ray photoelectron spectroscopy (XPS) measurements were carried out on an ESCALAB 250 spectrometer (Thermo Fisher Scientific, USA). X-ray diffraction (XRD) patterns were measured on a D/max 2500VL/PC diffractometer equipped with Cu K α line ($\lambda = 1.54060 \text{ \AA}$). Nitrogen sorption isotherms were carried out on a Micromeritics ASAP 2050 system. The surface area was determined according to Barret-Joyner-Halenda (BJH) model.

Electrochemical measurements: All electrochemical tests were performed on the CHI 760D electrochemical workstation (Chenhua Instrument Co., Ltd., Shanghai). During the test, a graphite rod was used as the counter electrode, Hg/HgO as the reference electrode, p-CoP/NF (0.5 cm \times 0.5 cm) as the working electrode and 1.0 M KOH as the electrolyte solution. The potential was referred to versus reversible hydrogen electrode (vs. RHE) by calibrating the reference electrode with Pt foil as both the working and the counter electrodes in a sealed standard three-electrode. Saturate the electrolyte with high-purity hydrogen for at least half an hour before performing electrode calibration. CV curve were performed at the scan rate of 1 mV s⁻¹ in 1.0 M KOH, as exhibited in Fig. S9. All potential data were recorded RHE using equation E-1, and the Tafel slope was estimated using equation E-2. Linear sweep voltammetry (LSV) was achieved in 1.0 M KOH at a scan rate of 2 mV s⁻¹. The potential cycling stability was measured by continuous cyclic voltammograms (CV) at a scan rate of 100 mV s⁻¹ with a range of overpotential of 0 to 0.2 V. Long-term stability was analysed via chronoamperometry.

$$E (\text{RHE}) = E (\text{Hg/HgO}) + 0.106 \text{ V} + 0.0591 \times \text{pH} - i \times R_s \quad (\text{E-1})$$

Where R_s is the solution impedance (Ω) and i is the current (A). Besides, the value of pH for 1.0 M KOH is 13.89.

$$\eta = a + b \times \log j \quad (\text{E-2})$$

Where η is the overpotential, b is the Tafel slope and j is the geometric current density. The E-3 and E-4 equations are used to calculate the number of active sites and turnover. Calculation of the number of active sites and turnover frequency (TOF)

The number of active sites (n) was determined by CV collected from -0.2 to +0.6 V vs. RHE in 1.0 M phosphate buffer solution (PBS, pH = 7) with a scan rate of 50 mV·s⁻¹. While it is difficult to assign the observed peaks to a given redox couple, n should be proportional to the integrated charge over the whole potential range. Assuming a one-electron process for both reduction and oxidation, the upper limit of n could be calculated with the equation (E-3):

$$n = \frac{Q}{2F} \quad (\text{E-3})$$

TOF can be calculated with the equation (E-4):

$$\text{TOF} = \frac{I}{2Fn} \quad (\text{E-4})$$

Where Q is the voltammetric charge, F is the Faraday constant (96485 C·mol⁻¹), I is the current (A) during the linear sweep measurement and n is the numbers of active sites (mol). The factor 1/2 in the equation represents that two electrons are required to form one hydrogen molecule from two protons. In addition, it is 1/4 for oxygen evolution reaction.

The electrochemically active surface area (ECSA) was evaluated according to the equation (E-5).

$$\text{ECSA} = \frac{C_{dl} \times S}{C_s} \quad (\text{E-5})$$

Where S is the actual surface area of the electrode, and C_s is the specific capacitance of an atomically smooth material. Therefore, C_s was considered to be a constant of 40 $\mu\text{F cm}^{-2}$ in this work. However, due to the approximate treatment of C_s , it is worth noting

that calculated ECSA could only be considered as approximate guide due to the inherent inaccuracies in its determination. The ECSA values of p-CoP/NF, CoP/NF, Co(OH)F/NF and NF are estimated to be 387.5, 225.0, 93.8 and 25.0 cm², respectively. The faradaic efficiency (FE) is calculated by E-6 equation.

$$FE = \frac{V_{\text{experiment}} \times NF}{V_m \times Q} \quad (\text{E-6})$$

Where the $V_{\text{experiment}}$ is the volume of gas actually collected, N is the number of transferred electrons, F is the faraday constant (96485 C mol⁻¹), Q is the charge passed through the electrode and V_m is the gas molar volume at 298 K and 101 kPa (24.5 L mol⁻¹).

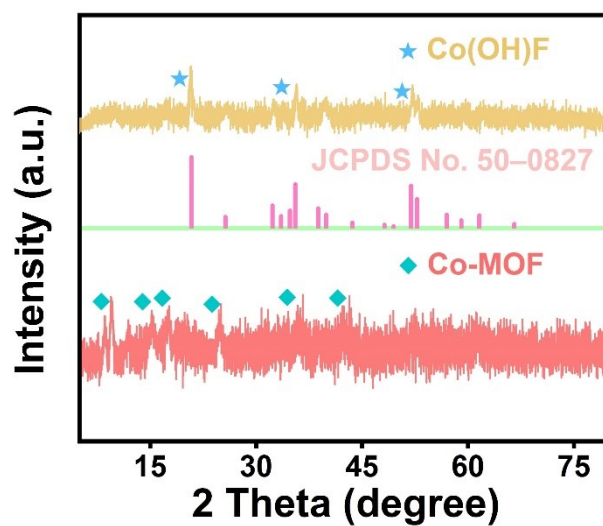


Fig. S1. XRD pattern of Co(OH)F and Co-MOF (The powder was obtained by continuous ultrasound for 1 h for testing).

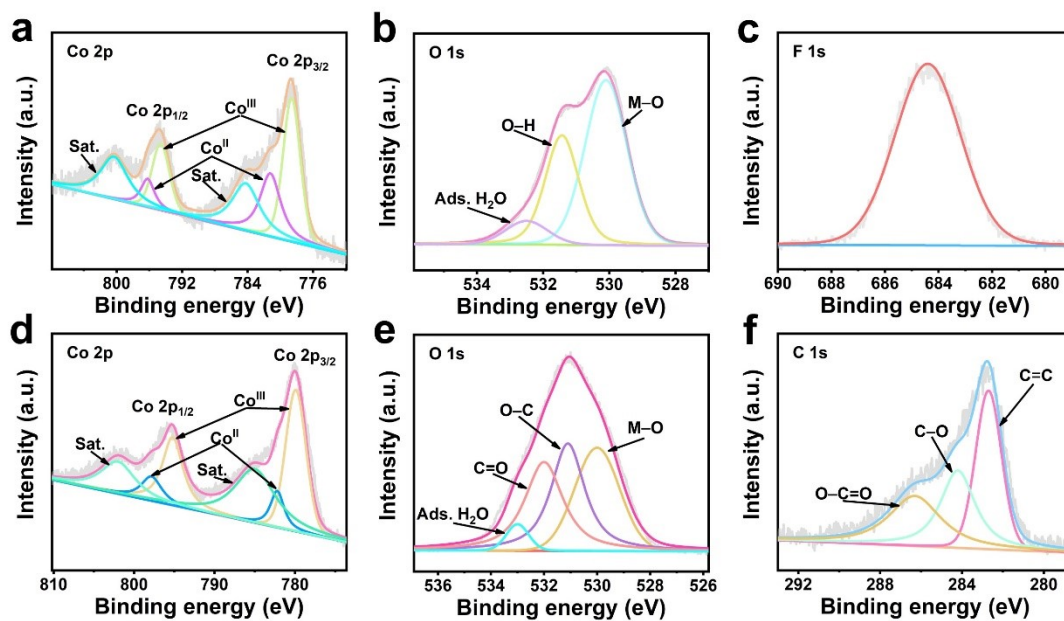


Fig. S2. High-resolution XPS spectra of Co(OH)F (a) Co 2p, (b) O 1s and (c) F 1s; High-resolution XPS spectra of Co-MOF (d) Co 2p, (e) O 1s and (f) C 1s.

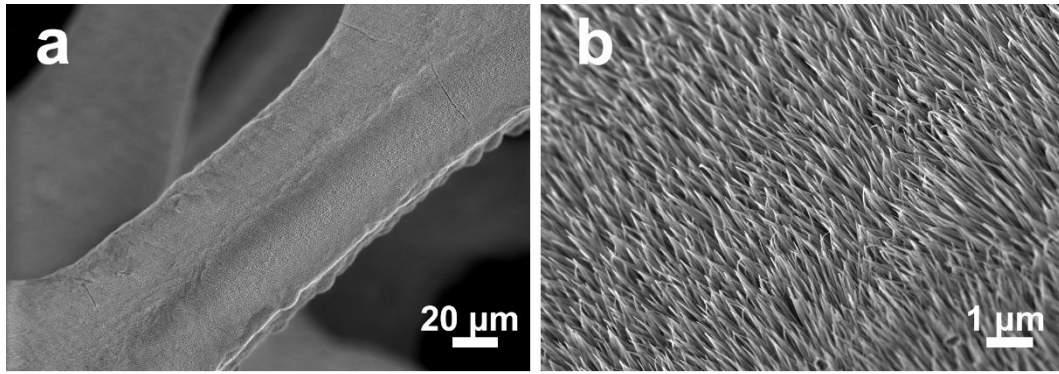


Fig. S3. (a,b) SEM images of Co(OH)F/NF.

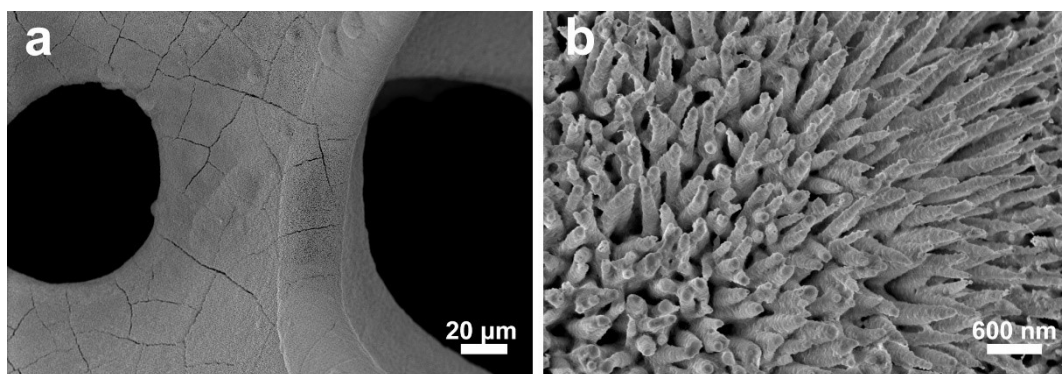


Fig. S4. (a,b) SEM images of Co-MOF/NF.

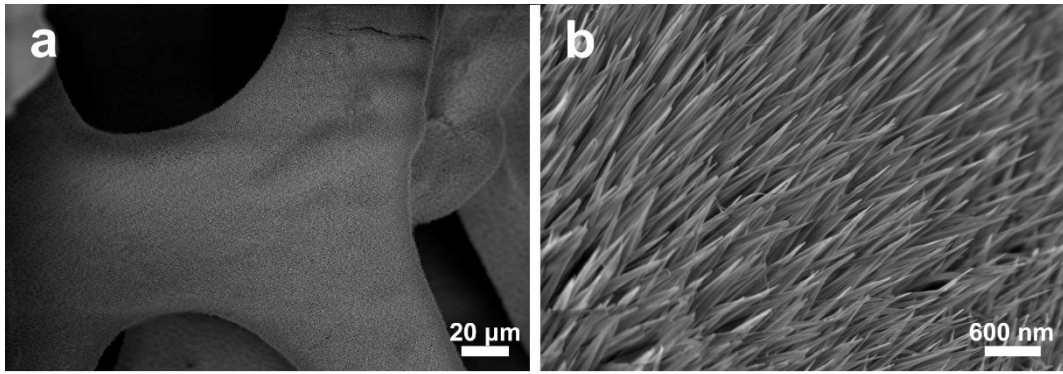


Fig. S5. (a,b) SEM images of CoP/NF.

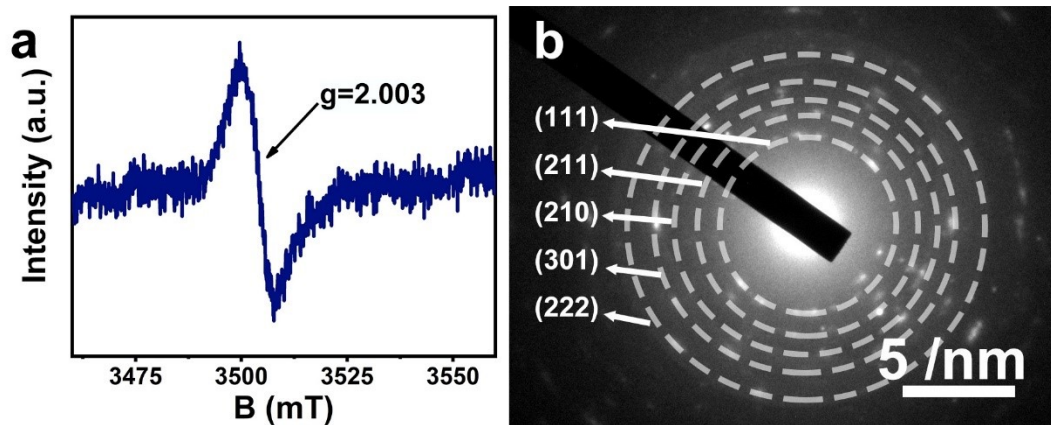


Fig. S6. (a) Room-temperature EPR spectra of p-CoP; (b) SAED pattern of p-CoP.

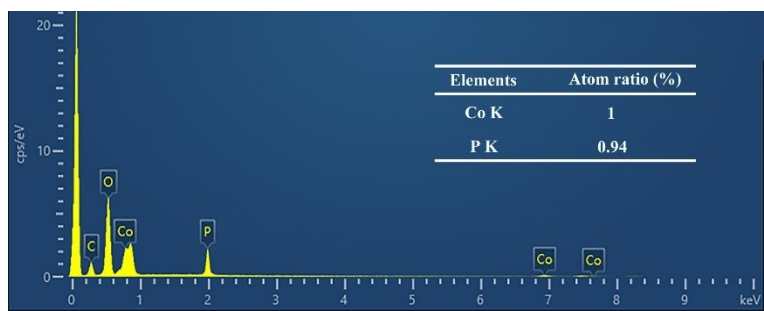


Fig. S7. Energy-dispersive X-ray spectrum of p-CoP/NF.

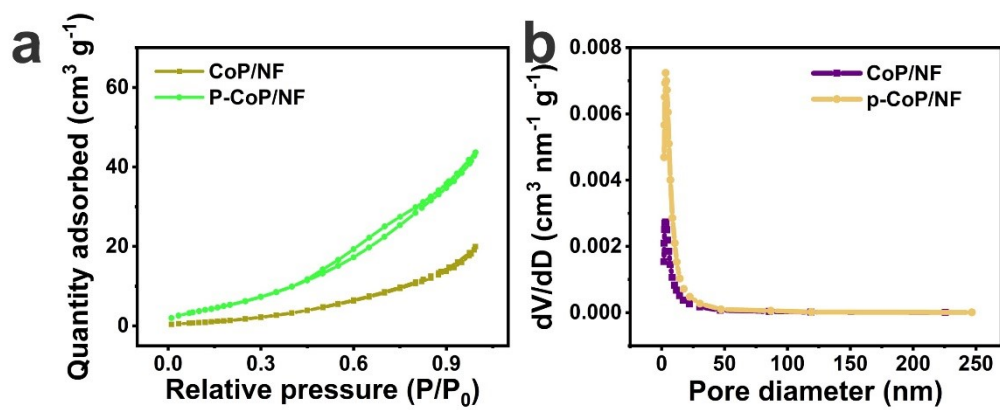


Fig. S8. (a) N₂ sorption isotherms; (b) pore size distribution of CoP/NF and p-CoP/NF.

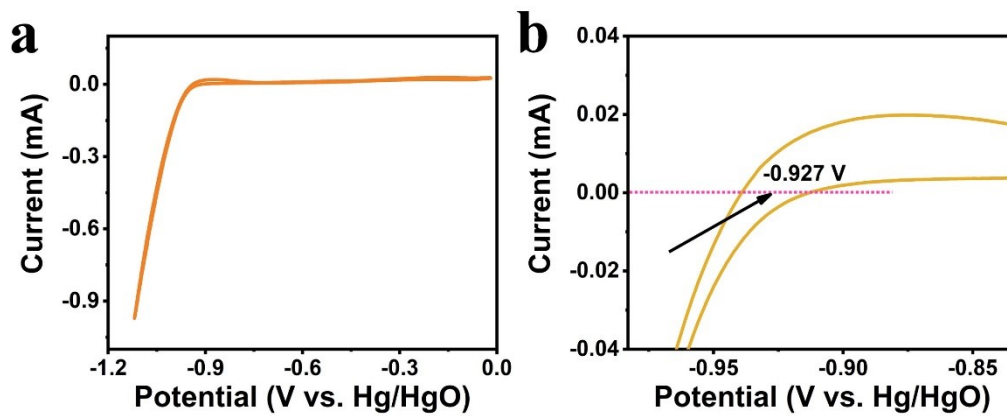


Fig. S9. (a) CV curve of Hg/HgO electrode calibration in 1.0 M KOH and (b) The enlarged view of (a).

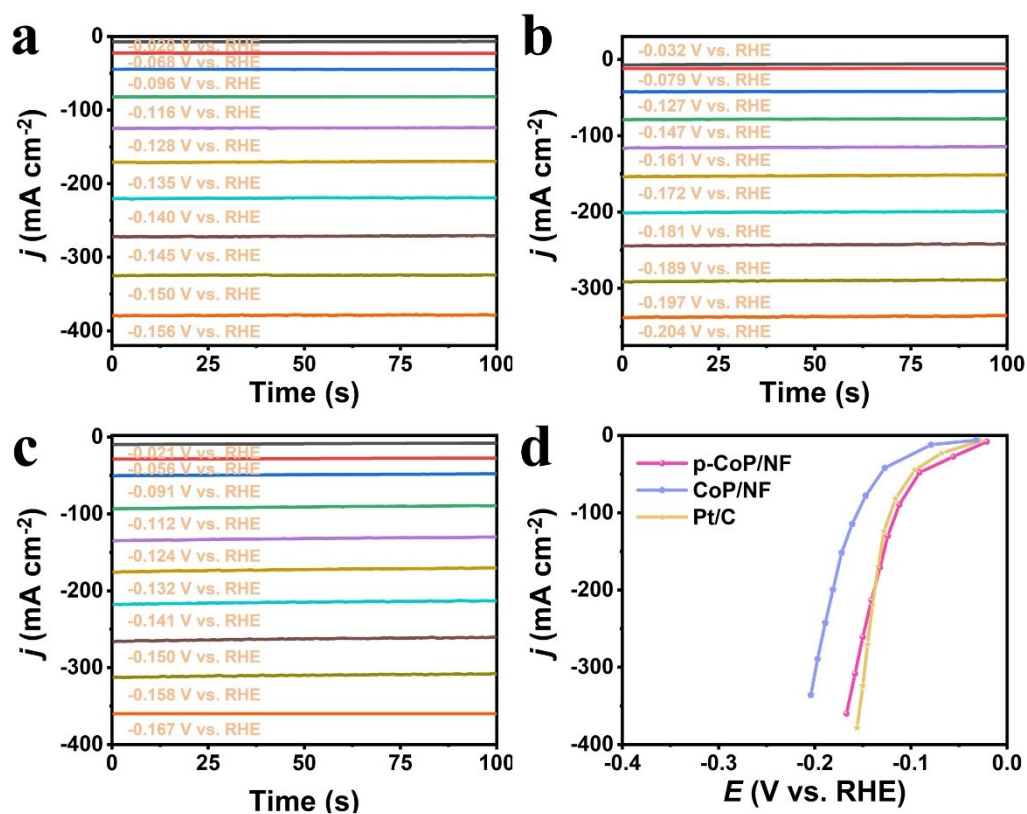


Fig. S10. CA responses of activity stabilized of (a) p-CoP/NF, (b) CoP/NF and (c) Pt/C in 1.0 M KOH in the catalytic turnover region. All potential data were iR-compensation; (d) True steady-state polarization curve constructed from HER current densities at the 100th second of CA responses.

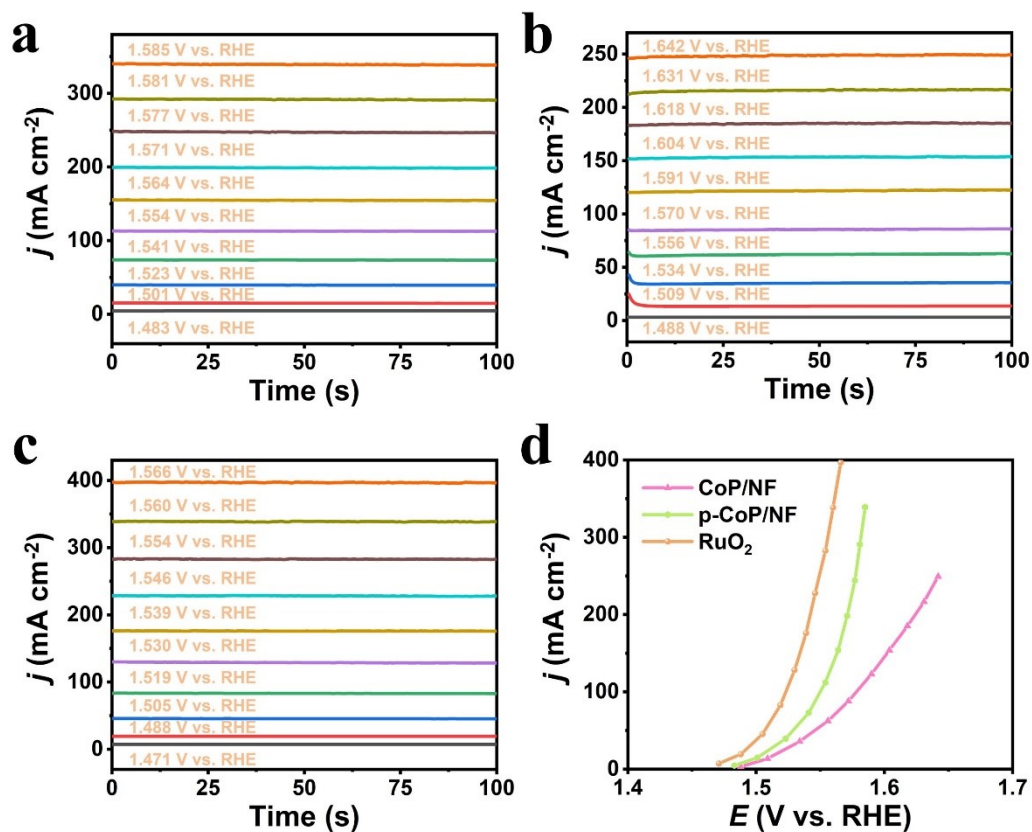


Fig. S11. CA responses of activity stabilized of (a) p-CoP/NF, (b) CoP/NF and (c) RuO₂ in 1.0 M KOH in the catalytic turnover region. All potential data were iR-compensation; (d) True steady-state polarization curve constructed from OER current densities at the 100th second of CA responses.

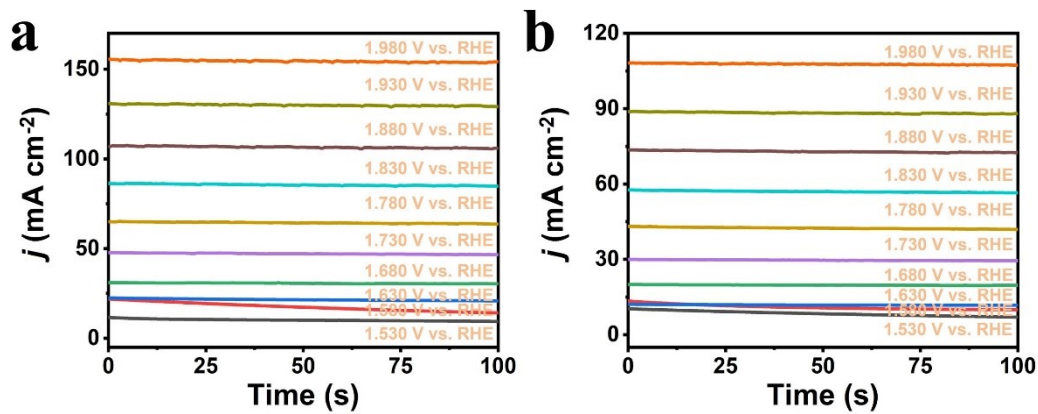


Fig. S12. CA responses of activity stabilized of (a) p-CoP/NF||p-CoP/NF and (b) CoP/NF||CoP/NF in 1.0 M KOH in the catalytic turnover region. All potential data were iR- compensation.

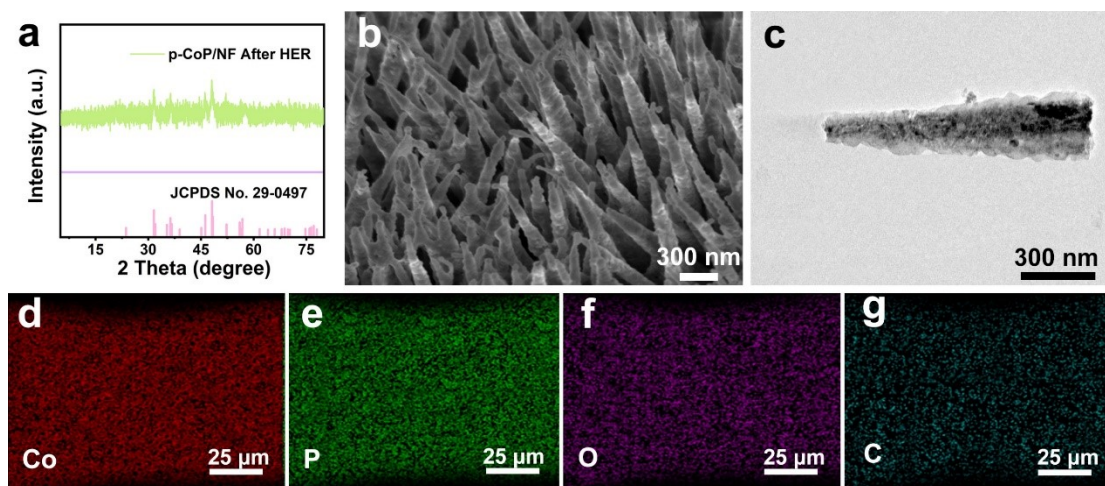


Fig. S13. (a) XRD (The powder was obtained by continuous ultrasound for 1 h for testing), (b) SEM, (c) TEM and (d-g) EDX elemental mapping images for p-CoP/NF after 15 h HER test.

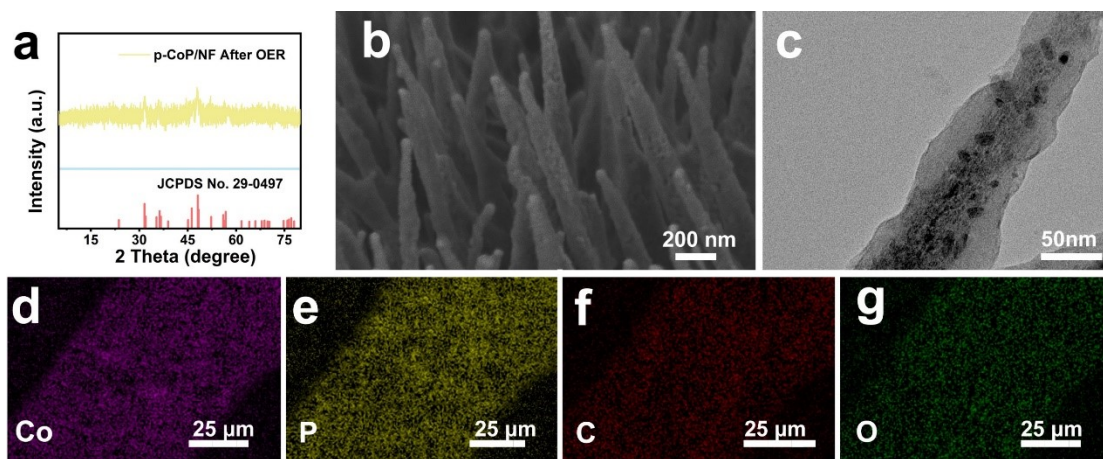


Fig. S14. (a) XRD (The powder was obtained by continuous ultrasound for 1 h for testing), (b) SEM, (c) TEM and (d-g) EDX elemental mapping images for p-CoP/NF after 15 h OER test.

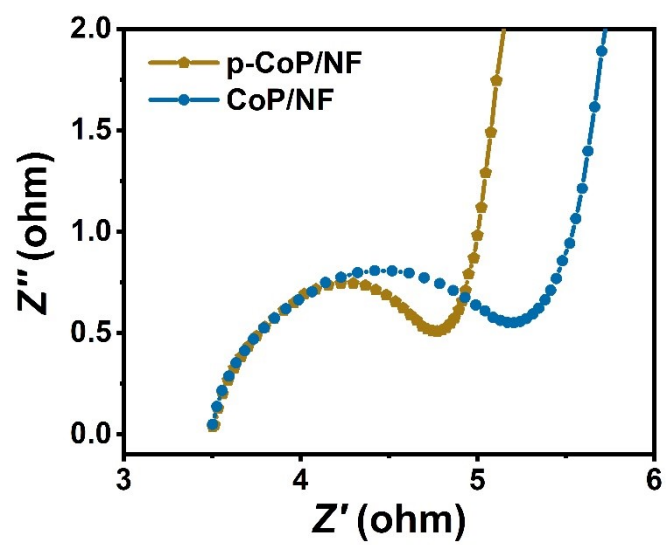


Fig. S15. Nyquist plots of p-CoP/NF and CoP/NF obtained at open circuit potential.

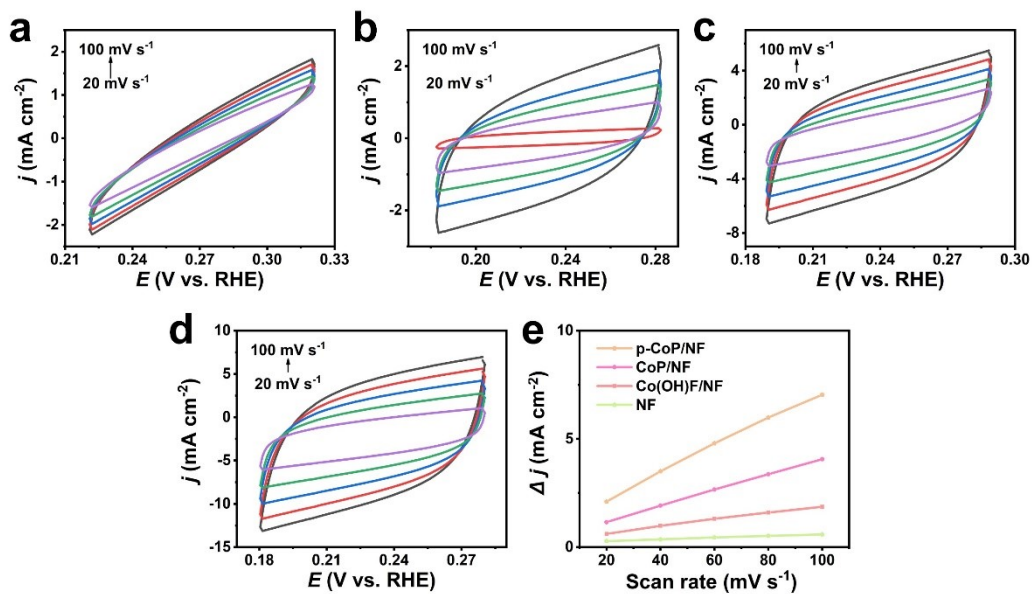


Fig. S16. CVs of (a) NF (b) Co(OH)F/NF, (c) CoP/NF and (d) p-CoP/NF under different scan rates; (e) Linear fitting curves of the capacitive currents vs. scan rates.

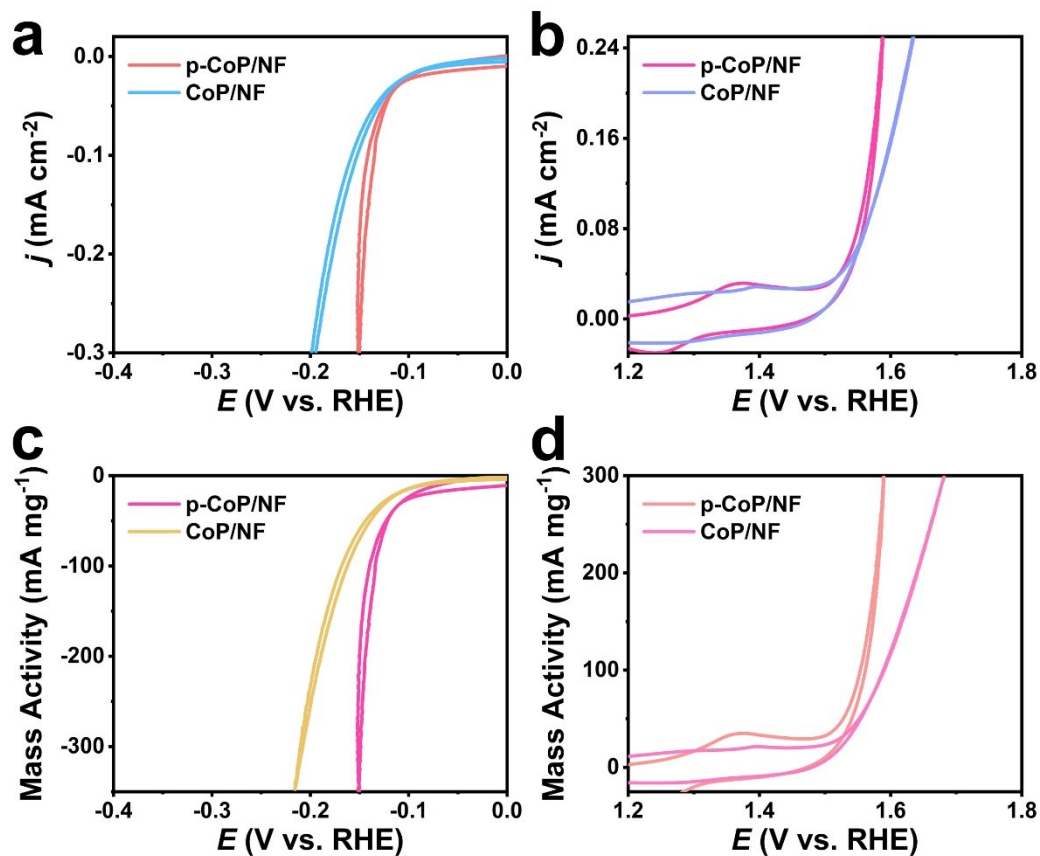


Fig. S17. (a) Electrochemical surface area is normalized HER polarization curves; (b) Electrochemical surface area is normalized OER polarization curves; (c) Mass loading is normalized HER polarization curves; (d) Mass loading is normalized OER polarization curves.

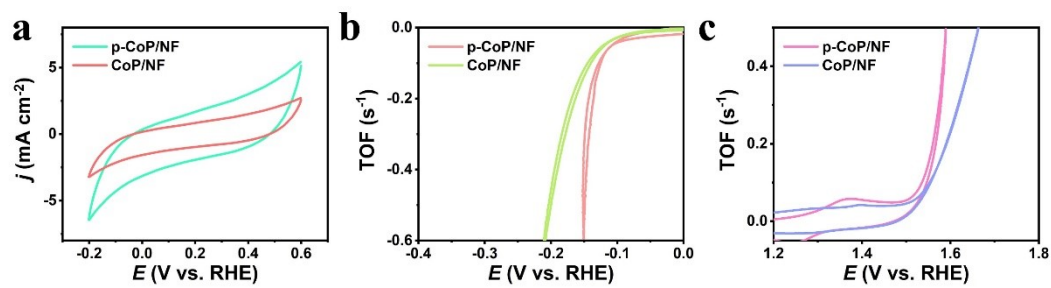


Fig. S18. (a) CV curves of p-CoP/NF and CoP/NF 1.0 M phosphate buffer solution (PBS, pH = 7) with a scan rate of 50 mV s⁻¹; TOF values of p-CoP/NF and CoP/NF (b) HER and (c) OER.

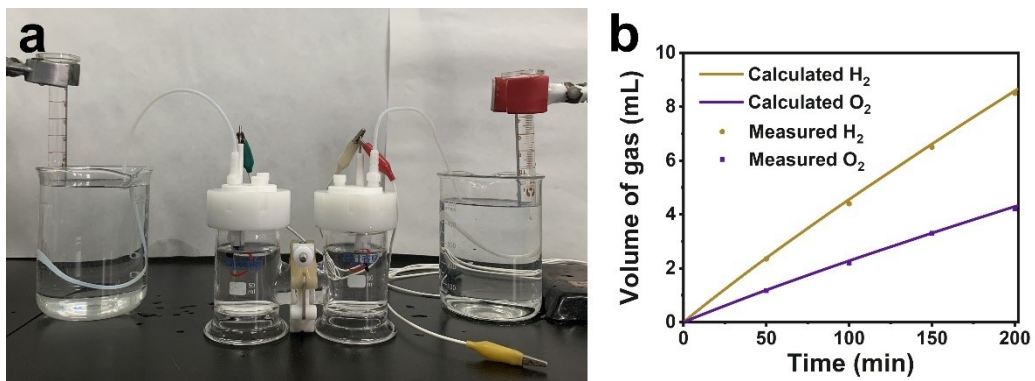


Fig. S19. (a) Gas collection device for gas; (b) The volume of gas, including calculated theoretically and measured experimentally.

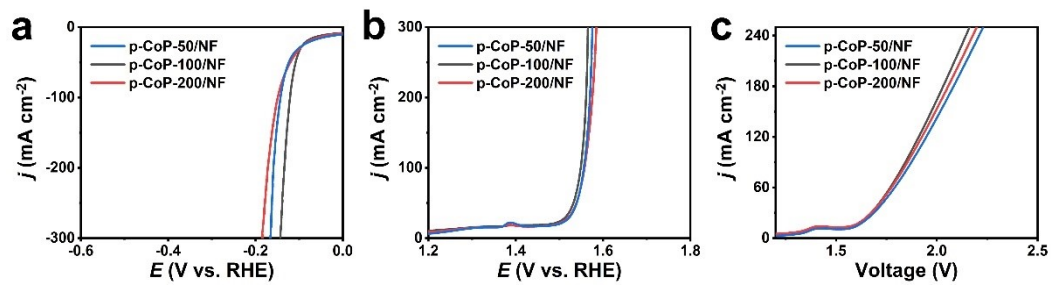


Fig. S20. (a) HER, (b) OER and (c) overall water splitting performances of p-CoP/NF (different quantity of p-phthalic acid (50, 100, 200 mg)).

Table S1. Comparison of the HER performance for p-CoP/NF with other catalysts.

Catalysts	Electrolyte	j (mA cm ⁻²)	η at the corresponding j (mV)	Tafel slope (mV dec ⁻¹)	Ref.
p-CoP/NF	1.0 M KOH	10	35	43	This work
CoP/NCNT-CP	1.0 M KOH	10	165	96	1
CoP NFs	1.0 M KOH	10	136	56.2	2
NiCoP/CNF	1.0 M KOH	10	130	83	3
Ni-Co-P	1.0 M KOH	10	121	65	4
CoP@NPC	1.0 M KOH	10	86	62.3	5
Bi/CoP	1.0 M KOH	10	122	60.2	6
NC-CNT/CoP	1.0 M KOH	10	120	73	7
Fe ₁ -NiCoP	1.0 M KOH	10	60	51.1	8
CoP-A	1.0 M KOH	10	100	76	9
CoP@FeCoP	1.0 M KOH	10	141	56.34	10
CuCo ₂ -P	1.0 M KOH	10	49.5	58	11
O-doped Co ₂ P/CuO NWs	1.0 M KOH	10	116	59	12
Co-Fe-P	1.0 M KOH	10	86	66	13
CoP/NCNHP	1.0 M KOH	10	115	66	14
CoP/NPC/TF	1.0 M KOH	10	80	50	15
CoP/Co ₂ P	1.0 M KOH	10	68	51.8	16

Table S2. Comparison of the OER performance for p-CoP/NF with other catalysts.

Catalysts	Electrolyte	j (mA cm ⁻²)	η at the corresponding j (mV)	Tafel slope (mV dec ⁻¹)	Ref.
p-CoP/NF	1.0 M KOH	10	253	59	This work
O-doped Co ₂ P/CuO NWs/CF	1.0 M KOH	10	270	74.4	12
CoP/NCNHP	1.0 M KOH	10	310	70	14
NiCoFeP/C	1.0 M KOH	10	270	65	17
Er doped CoP	1.0 M KOH	20	256	70	18
NiCoP@NC NA/NF	1.0 M KOH	50	305	70.5	19
CoP@NG	1.0 M KOH	10	354	63.8	20
Ni-CoP@C	1.0 M KOH	10	279	54	21
Fe-CoP cage	1.0 M KOH	10	300	35.2	22
CoP-TiOx	1.0 M KOH	10	337	72.1	23
CoP ₂ /Fe-CoP ₂ YSB	1.0 M KOH	10	266	68.1	24
CoP@NiCo-LDH	1.0 M KOH	20	271	98	25
MnO ₂ -CoP ₃ /Ti	1.0 M KOH	10	288	65	26
CoP ₂ @3D-NPC	1.0 M KOH	20	372	67	27
CoP-B1	1.0 M KOH	10	297	58.1	28

Table S3. Comparison of the overall water splitting activity for p-CoP/NF with other catalysts.

Catalysts	Electrolyte	j (mA cm ⁻²)	Voltage at the corresponding j (mV)	Ref.
p-CoP/NF	1.0 M KOH	10	1.55	This work
CoP@NPC	1.0 M KOH	10	1.60	5
Fe ₁ -NiCoP	1.0 M KOH	10	1.61	8
CoP@FeCoP	1.0 M KOH	10	1.68	10
CoP/NCNHP	1.0 M KOH	20	1.64	14
CoP/Co ₂ P	1.0 M KOH	10	1.57	16
Er doped CoP	1.0 M KOH	10	1.58	18
CoP NA/CC	1.0 M KOH	10	1.65	29
CoP NFs	1.0 M KOH	50	1.65	30
CoP/rGO-400	1.0 M KOH	10	1.70	31
V-CoP@a-CeO ₂	1.0 M KOH	10	1.56	32
FeCoP UNSAs	1.0 M KOH	10	1.60	33
CoP-N/Co foam	1.0 M KOH	10	1.61	34

References

1. L. Wang, J. Cao, X. Cheng, C. Lei, Q. Dai, B. Yang, Z. Li, M. A. Younis, L. Lei, Y. Hou and K. Ostrikov, *ACS Sustain. Chem. Eng.*, 2019, **7**, 10044–10051.
2. L. Ji, J. Wang, X. Teng, T. J. Meyer and Z. Chen, *ACS Catal.*, 2019, **10**, 412–419.
3. S. Surendran, S. Shanmugapriya, A. Sivanantham, S. Shanmugam and R. Kalai Selvan, *Adv. Energy Mater.*, 2018, **8**, 1800555.
4. X. Liu, S. Deng, D. Xiao, M. Gong, J. Liang, T. Zhao, T. Shen and D. Wang, *ACS Appl. Mater. Interfaces*, 2019, **11**, 42233–42242.
5. Z. Chen, H. Jia, J. Yuan, X. Liu, C. Fang, Y. Fan, C. Cao and Z. Chen, *Int. J. Hydrog. Energy*, 2019, **44**, 24342–24352.
6. L. Guo, X. Bai, H. Xue, J. Sun, T. Song, S. Zhang, L. Qin, K. Huang, F. He and Q. Wang, *Chem. Commun.*, 2020, **56**, 7702–7705.
7. C. Guan, H. Wu, W. Ren, C. Yang, X. Liu, X. Ouyang, Z. Song, Y. Zhang, S. J. Pennycook, C. Cheng and J. Wang, *J. Mater. Chem. A*, 2018, **6**, 9009–9018.
8. M. Guo, S. Song, S. Zhang, Y. Yan, K. Zhan, J. Yang and B. Zhao, *ACS Sustain. Chem. Eng.*, 2020, **8**, 7436–7444.
9. L. Su, X. Cui, T. He, L. Zeng, H. Tian, Y. Song, K. Qi and B. Y. Xia, *Chem. Sci.*, 2019, **10**, 2019–2024.
10. J. Shi, F. Qiu, W. Yuan, M. Guo and Z. Lu, *Chem. Eng. J.*, 2021, **403**, 126312.
11. Y. Cheng, Y. Pei, P. Zhuang, H. Chu, Y. Cao, W. Smith, P. Dong, J. Shen, M. Ye and P. M. Ajayan, *Small*, 2019, **15**, 1904681.
12. T. L. Luyen Doan, D. T. Tran, D. C. Nguyen, H. Tuan Le, N. H. Kim and J. H. Lee, *Appl. Catal. B: Environ.*, 2020, **261**, 118268.
13. J. Chen, J. Liu, J. Xie, H. Ye, X. Fu, R. Sun and C. Wong, *Nano Energy*, 2019, **56**, 225–233.
14. Y. Pan, K. Sun, S. Liu, X. Cao, K. Wu, W. Cheong, Z. Chen, Y. Wang, Y. Li, Y. Liu, D. Wang, Q. Peng, C. Chen and Y. Li, *J. Am. Chem. Soc.*, 2018, **140**, 2610–2618.

15. X. Huang, X. Xu, C. Li, D. Wu, D. Cheng and D. Cao, *Adv. Energy Mater.*, 2019, **9**, 1803970.
16. Y. Hua, Q. Xu, Y. Hu, H. Jiang and C. Li, *J. Energy Chem.*, 2019, **37**, 1–6.
17. X. Wei, Y. Zhang, H. He, L. Peng, S. Xiao, S. Yao and P. Xiao, *Chem. Commun.*, 2019, **55**, 10896–10899.
18. G. Zhang, B. Wang, J. Bi, D. Fang and S. Yang, *J. Mater. Chem. A*, 2019, **7**, 5769–5778.
19. B. Cao, Y. Cheng, M. Hu, P. Jing, Z. Ma, B. Liu, R. Gao and J. Zhang, *Adv. Funct. Mater.*, 2019, **29**, 1906316.
20. Y. Lu, W. Hou, D. Yang and Y. Chen, *Electrochim. Acta*, 2019, **307**, 543–552.
21. X. Han, C. Yu, H. Huang, W. Guo, C. Zhao, H. Huang, S. Li, Z. Liu, X. Tan, Z. Gao, J. Yu and J. Qiu, *Nano Energy*, 2019, **62**, 136–143.
22. J. Xie, Z. Liu, J. Li, L. Feng, M. Yang, Y. Ma, D. Liu, L. Wang, Y. Chai and B. Dong, *J. Energy Chem.*, 2020, **48**, 328–333.
23. Z. Liang, W. Zhou, S. Gao, R. Zhao, H. Zhang, Y. Tang, J. Cheng, T. Qiu, B. Zhu, C. Qu, W. Guo, Q. Wang and R. Zou, *Small*, 2020, **16**, 1905075.
24. V. Ganesan, J. Son and J. Kim, *Nanoscale*, 2021, **13**, 4569–4575.
25. W. Tian, J. Zhang, H. Feng, H. Wen, X. Sun, X. Guan, D. Zheng, J. Liao, M. Yan and Y. Yao, *Sustain. Energy Fuels*, 2021, **5**, 391–395.
26. X. Xiong, Y. Ji, M. Xie, C. You, L. Yang, Z. Liu, A. M. Asiri and X. Sun, *Electrochem. commun.*, 2018, **86**, 161–165.
27. S. Yang, M. Xie, L. Chen, W. Wei, X. Lv, Y. Xu, N. Ullah, O. C. Judith, Y. B. Adegbemiga and J. Xie, *Int. J. Hydrog. Energy*, 2019, **44**, 4543–4552.
28. G. Yuan, J. Bai, L. Zhang, X. Chen and L. Ren, *Appl. Catal. B: Environ.*, 2021, **284**, 119693.
29. T. Liu, L. Xie, J. Yang, R. Kong, G. Du, A. M. Asiri, X. Sun and L. Chen, *ChemElectroChem*, 2017, **4**, 1840–1845.
30. L. Ji, J. Wang, X. Teng, T. J. Meyer and Z. Chen, *ACS Catal.*, 2020, **10**, 412–419.
31. L. Jiao, Y. Zhou and H. Jiang, *Chem. Sci.*, 2016, **7**, 1690–1695.
32. L. Yang, R. Liu and L. Jiao, *Adv. Funct. Mater.*, 2020, **30**, 1909618.

33. L. Zhou, M. Shao, J. Li, S. Jiang, M. Wei and X. Duan, *Nano Energy*, 2017, **41**, 583–590.
34. Z. Liu, X. Yu, H. Xue and L. Feng, *J. Mater. Chem. A*, 2019, **7**, 13242–13248.